Near-zero thermal expansion in β-$CuZnV_2O_7$ in a large temperature range

Yaguang Hao(郝亚光), Hengli Xie(谢恒立), Gaojie Zeng(曾高杰), Huanli Yuan(袁焕丽), Yangming Hu(胡杨明), Juan Guo(郭娟), Qilong Gao(高其龙), Mingju Chao(晁明举), Xiao Ren(任霄), and Er-Jun Liang(梁二军)
Citation: Chin. Phys. B, 2022, 31 (**4**): 046502. DOI: 10.1088/1674-1056/ac3393
Journal homepage: http://cpb.iphy.ac.cn; http://iopscience.iop.org/cpb

What follows is a list of articles you may be interested in

Zero thermal expansion in metal-organic framework with imidazole dicarboxylate ligands

Qilong Gao(高其龙), Yixin Jiao(焦怡馨), and Gang Li(李纲)
Chin. Phys. B, 2022, 31 (**4**): 046501. DOI: 10.1088/1674-1056/ac3ecf

Negative thermal expansion in NbF_3 and $NbOF_2$: A comparative theoretical study

Mingyue Zhang(张明月), Chunyan Wang(王春艳), Yinuo Zhang(张一诺), Qilong Gao(高其龙), and Yu Jia(贾瑜)
Chin. Phys. B, 2021, 30 (**5**): 056501. DOI: 10.1088/1674-1056/abe376

Low thermal expansion and broad band photoluminescence of $Zr_{0.1}Al_{1.9}Mo_{2.9}V_{0.1}O_{12}$

Jun-Ping Wang(王俊平), Qing-Dong Chen(陈庆东), Li-Gang Chen(陈立刚), Yan-Jun Ji(纪延俊), You-Wen Liu(刘友文), and Er-Jun Liang(梁二军)
Chin. Phys. B, 2021, 30 (**3**): 036501. DOI: 10.1088/1674-1056/abcf39

Phase transition and near-zero thermal expansion of $Zr_{0.5}Hf_{0.5}VPO_7$

Jun-Ping Wang(王俊平), Qing-Dong Chen(陈庆东), Sai-Lei Li(李赛磊), Yan-Jun Ji(纪延俊), Wen-Ying Mu(穆文英), Wei-Wei Feng(冯伟伟), Gao-Jie Zeng(曾高杰), You-Wen Liu(刘友文), Er-Jun Liang(梁二军)
Chin. Phys. B, 2018, 27 (**6**): 066501. DOI: 10.1088/1674-1056/27/6/066501

Near-zero thermal expansion of $In_{2(1-x)}(HfMg)_xMo_3O_{12}$ with tailored phase transition

Yong-Guang Cheng(程永光), Yan-Chao Mao(毛彦超), Xain-Sheng Liu(刘献省), Bao-He Yuan(袁保合), Ming-Ju Chao(晁明举), Er-Jun Liang(梁二军)
Chin. Phys. B, 2016, 25 (**8**): 086501. DOI: 10.1088/1674-1056/25/8/086501

Near-zero thermal expansion in β-$CuZnV_2O_7$ in a large temperature range

Yaguang Hao(郝亚光), Hengli Xie(谢恒立), Gaojie Zeng(曾高杰), Huanli Yuan(袁焕丽), Yangming Hu(胡杨明), Juan Guo(郭娟), Qilong Gao(高其龙), Mingju Chao(晁明举), Xiao Ren(任霄)[†], and Er-Jun Liang(梁二军)[‡]

Key Laboratory of Materials Physics of Ministry of Education, and School of Physics and Microelectronics, Zhengzhou University, Zhengzhou 450052, *China*

(Received 18 September 2021; revised manuscript received 19 October 2021; accepted manuscript online 27 October 2021)

We report a new type of near-zero thermal expansion material β-$CuZnV_2O_7$ in a large temperature range from 173 K to 673 K. It belongs to a monoclinic structure ($C2/c$ space group) in the whole temperature range. No structural phase transition is observed at atmospheric pressure based on the x-ray diffraction and Raman experiment. The high-pressure Raman experiment demonstrates that two structural phase transitions exist at 0.94 GPa and 6.53 GPa, respectively. The mechanism of negative thermal expansion in β-$CuZnV_2O_7$ is interpreted by the variations of the angles between atoms intuitively and the phonon anharmonicity intrinsically resorting to the negative Grüneisen parameter.

Keywords: negative thermal expansion materials, β-$CuZnV_2O_7$, expansion mechanism, Raman spectrum

PACS: 65.40.De, 61.66.–f, 62.50.–p, 33.20.Fb **DOI:** 10.1088/1674-1056/ac3393

1. Introduction

Negative thermal expansion (NTE) materials are a series of abnormal materials with volumes reducing as the temperature rises.[1,2] This abnormal temperature behavior of NTE materials takes great advantages in the applications of precise instruments, especially extending the service time and optimizing the performance, resorting to the restraint of volume changes when temperature varies. NTE materials, especially the near-zero NTE material with a low NTE coefficient which is the best choice but very rare, provide a good chance to overcome the mismatch of thermal expansion coefficients between materials as temperature varies. Many oxide NTE materials have excellent NTE properties such as $ZrMnMo_3O_{12}$, $Sc_{2-x}Ga_xW_3O_{12}$ and Ca_2RuO_4 with oxygen vacancy.[3–5] Nevertheless, many challenges remain[6,7] such as the hydroscopicity[8,9] and the limited NTE temperature range attributed to the structural phase transition.[10,11] Just like ZrW_2O_8, a well-known NTE material relying on frame structure to induce NTE property,[12] the family of vanadate with the chemical formulae of AV_2O_7 (A = Zr, Hf)[13–16] and $B_2V_2O_7$ (B = Cu, Zn)[17–21] also shows distinct advantages of NTE characteristics. Apart from vanadate, phosphate, especially α-$Cu_2P_2O_7$ (space group $C2/c$), also displays high NTE properties along the a and b axes with the volume expansion coefficient $\alpha_v = -27.69 \times 10^{-6}$ K^{-1}.[22] The parent compounds of vanadate display the NTE property in different temperature ranges, but their limited NTE temperature ranges and the uncontrollable NTE coefficients hinder their further applications. A mount of efforts has been made to enrich the kinds of NTE materials in vanadate, in which doping new elements to the A, V, and B sites were proven to be an efficient way to modulate the NTE property. For example, with the individual site substitution of V by P or V by Mo, it was turned out that the structural phase transition temperatures of $ZrV_{2-x}P_xO_7$ ($x = 1$) and $ZrV_{2-x}Mo_xO_7$ ($x = 0.5$) are successfully decreased to 231 K and 225 K, respectively, reducing the low limit of the NTE temperature of ZrV_2O_7, which is 375 K.[23,24] Moreover, doping new elements to the B site of $B_2V_2O_7$ (B = Cu, Zn), such as $Cu_{1.5}Mg_{0.5}V_2O_7$ and β-$Cu_{1.8}Zn_{0.2}V_2O_7$, could also broaden the NTE temperature range from 153 K–573 K to 100 K–700 K.[25,26]

In addition, doping new elements also plays an important role in regulating the NTE coefficient, especially to obtain the near-zero expansion materials. For the AV_2O_7 (A = Zr, Hf) vanadate, with the partial substitutions of Zr to Hf and V to P in ZrV_2O_7, the $Zr_{0.5}Hf_{0.5}VPO_7$ displays near-zero thermal expansion behavior with the volume expansion coefficient of $\alpha_v = -1.77 \times 10^{-6}$ K^{-1} in the temperature range of 310 K–673 K.[27] Like the $Zr_{0.5}Hf_{0.5}VPO_7$, with the partial substitutions of Zr by Fe and V by Mo in ZrV_2O_7, the $Zr_{0.1}Fe_{0.9}V_{1.1}Mo_{0.9}O_7$ shows near-zero thermal expansion property with the volume expansion coefficient of $\alpha_v = -2.53 \times 10^{-6}$ K^{-1} in the temperature range of 300 K–873 K.[28]

Nevertheless, the doped NTE materials mentioned above are all multi-site substitutions, which is not economical and high-efficiency. Actually, the compounds by individual substitution in the family of $B_2V_2O_7$ (B = Cu, Zn) have been suc-

[†]Corresponding author. E-mail: rxphy@zzu.edu.cn
[‡]Corresponding author. E-mail: ejliang@zzu.edu.cn

cessfully synthesized. With Cd partially doping to the Zn site in $Zn_2V_2O_7$, β-$Zn_{1.6}Cd_{0.4}V_2O_7$ behaves near-zero thermal expansion property with a broad temperature range of about 273 K–873 K.[29] However, the low limit of NTE temperature in β-$Zn_{1.6}Cd_{0.4}V_2O_7$ is just at 273 K, which cannot satisfy the further applications in low-temperature environment. Recently, the α-$Cu_{1.8}Zn_{0.2}V_2O_7$ obtained by single-site substitution through Cu by Zn displays near-zero NTE behavior from 100 K to 475 K,[30] attracting much attention. This temperature range involves room temperature and touches down below 273 K, which reveals that α-$Cu_{1.8}Zn_{0.2}V_2O_7$ could be a candidate for wide applications. Based on the fact that the volumetric NTEs of α-$Cu_{2-x}Zn_xV_2O_7$ ($x = 0$, 0.1, 0.2) is successfully tuned from -10.19×10^{-1} K^{-1} to -1.58×10^{-1} K^{-1} in the temperature range of 100 K–475 K, the content of Zn is considered to be a pivotal factor to modulate the NTE property of α-$Cu_{2-x}Zn_xV_2O_7$ usefully.[30]

Motivated by the fact in α-$Cu_2V_2O_7$, here we report a new type of near-zero thermal expansion material with a molecular formula of β-$CuZnV_2O_7$. This new kind of NTE material is acquired by doping the equivalent amount of Zn to the site of Cu in the parent compound of β-$Cu_2V_2O_7$, another stable phase of $Cu_2V_2O_7$ except α-$Cu_2V_2O_7$. The linear NTE coefficients of β-$CuZnV_2O_7$ are $\alpha_l = -2.15\times10^{-6}$ K^{-1} (173–325 K) and $\alpha_l = -0.72\times10^{-6}$ K^{-1} (325–673 K). The NTE temperature range of β-$CuZnV_2O_7$ is large enough to be over the 273 K and room temperature, which meets the needs for multiple applications. Apart from the NTE property, we also demonstrate that no structural phase transition exists in β-$CuZnV_2O_7$ from 173 K to 673 K by variable-temperature x-ray diffraction and Raman experiment at atmospheric pressure. However, two structural phase transitions are observed by the high-pressure Raman measurement.

2. Experimental

High quality polycrystal powder of β-$CuZnV_2O_7$ was prepared by the solid phase sintering reaction method. According to the chemical stoichiometry of $CuZnV_2O_7$, the raw materials CuO (99.0%), ZnO (99.0%), and V_2O_5 (99.0%) were ground in a mortar for about half an hour in advance. Then an appropriate amount of alcohol was added into the mixed powder and the mixture was stirred for 2–3 h. After fully grinding, the mixed powder was pressed into a cylinder shape with a diameter of 10 mm and a height of 8 mm by a tablet press (specification for 769YP-15A & 24B hydraulic press). Then the compressed cylinder was put into a box furnace (AY-TF-100-120) and heated to 873 K with a heating rate of 5 K/min, and sintered at 873 K for 4 h. Finally, the box furnace cooled down naturally and high quality polycrystal powder of β-$CuZnV_2O_7$ was obtained.

A temperature-dependent x-ray diffraction (XRD) data was collected using (Japan, Rigaku Corporation, Cu, K_α, $\lambda = 1.5418$ Å) x-ray diffractometer to measure the structural transformation of β-$CuZnV_2O_7$ from 80 K to 573 K. The x-ray diffraction data was analyzed by the Full-Prof software and Rietveld method refinement. A dilatometer (LINSEIS DIL L75) was used to test the thermal expansion property of β-$CuZnV_2O_7$ with heating and cooling rates of 5 K/min. The microstructure of the sample was observed by the scanning microscope (JSM-6700F). The Raman spectrum of the sample was measured by a Horiba Lab RAM HR Evolution Raman spectrometer ($\lambda = 633$ nm, 143–663 K) with a resolution as high as 0.6 cm^{-1} using 1800 gr/mm. High-pressure Raman measurement were carried out by the laser with a wavelength of 532 nm. The samples used in high-pressure Raman experiment were kept in a diamond anvil cell with a small number of rubies for pressure calibration and silicone oil was used as the pressure transmitting medium

3. Results and discussion

3.1. Structure analysis

Figure 1(a) shows the refined analysis of the XRD pattern at room temperature. The diffraction peaks of β-$CuZnV_2O_7$ could be well indexed according to the standard PDF card of β-$CuZnV_2O_7$. It belongs to a centrally symmetric monoclinic phase structure with the space group of $C2/c$ (No. 15). The unit cell parameters refined by the Rietveld method are $a = 7.54671$ Å, $b = 8.18740$ Å, $c = 10.10099$ Å, $\beta = 110.9198°$, and $V = 582.978$ Å^3. The R values are $R_p = 15.6$, $R_{wp} = 14.6$, and $R_{exp} = 8.53$, verifying the accuracy of the fitting result. According to our refined XRD result, the schematic of framework structure of β-$CuZnV_2O_7$ could be presented as the model shown in Fig. 1(b). This model is consistent with the schematic structure of β-$Cu_2V_2O_7$, which holds the same structure of β-$CuZnV_2O_7$.[18] In Fig. 1(b), two VO_4 tetrahedrons form the V_2O_7 double tetrahedron structure unit by sharing one oxygen atom at the same vertex angle.

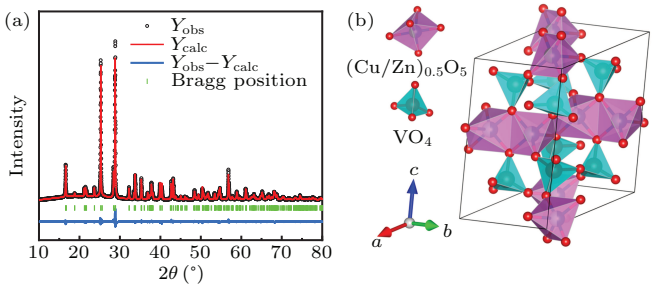

Fig. 1. (a) Rietveld refined analysis of XRD data of β-$CuZnV_2O_7$ at room temperature. (b) Rietveld refined structure of β-$CuZnV_2O_7$.

Each V_2O_7 block possesses a staggered Cs symmetric structure.[31] The $(CuZn)_{0.5}O_5$ quadrangular pyramid is composed of one Cu/Zn and five O, and two quadrangular pyramids share one side. Due to the Jahn–Teller distortion effect,

a distorted quadrangular pyramid chain is formed.[31,32] The distorted tetragonal pyramid chain is connected to the V_2O_7 double tetrahedron by sharing the apex oxygen atom to form a chain, forming a layered staggered structure.[31,32]

3.2. Morphology and composition

The SEM image of the sample can be seen from Fig. 2(a), and particles in the polycrystal powder of β-$CuZnV_2O_7$ are relatively smooth with the diameter of each particle about 1–2 μm. The population distribution of particles is relatively dense except for fewer tiny voids, holes, and micro-cracks remaining among the particles. To determine the composition of the material elements, the EDS spectrum of the sample was tested [Fig. 2(b)]. The analysis of the EDS energy spectrum composition (atomic fraction at.%, mass fraction wt.%) is shown in Table 1, and the element content ratio of Cu:Zn:V:O meets the ratio of the chemical formula of β-$CuZnV_2O_7$ within the allowable error range.

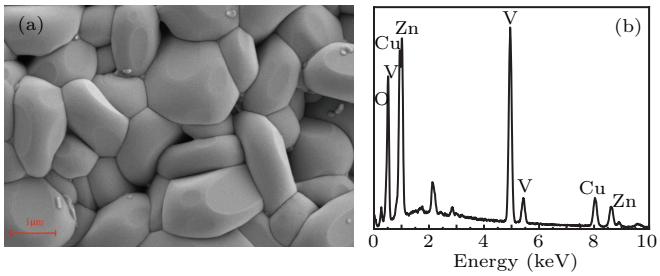

Fig. 2. (a) SEM image of β-$CuZnV_2O_7$ sample, (b) the EDS spectrum in (a).

Table 1. Composition analysis of β-$CuZnV_2O_7$ EDS (atomic fraction at.%, mass fraction wt.%).

Element	Cu	Zn	V	O
at.%	13.30	15.69	26.79	44.22
wt.%	21.43	26.01	34.62	17.94

3.3. Thermal expansion performance and no structural phase transition at atmospheric pressure

The temperature-dependent x-ray diffraction pattern of β-$CuZnV_2O_7$ at atmospheric pressure is shown in Fig. 3(a). All diffraction peaks show normal temperature-dependent behavior from 80 K to 573 K, with no anomalies being observed, which indicates that the crystal structure of β-$CuZnV_2O_7$ remains unchanged. Figures 3(b) and 3(c) are partially enlarged views of two diffraction peaks indexed by [002] and [200]. The shifts to the high angle of these two diffraction peaks demonstrate the contraction of the c and a axes with temperature rising.

According to the Rietveld refinement result of XRD data obtained by Fullprof software, the a and c axes gradually decrease upon temperature rising (Fig. 4(a)), which is in sync with the changes as shown in Figs. 3(b) and 3(c). However, the b axis is just the reverse. According to the data in Fig. 4(a), the thermal expansion coefficients of a, b, and c axis are $\alpha_a = -2.7 \times 10^{-7}$ K^{-1}, $\alpha_b = 4.4 \times 10^{-6}$ K^{-1} and $\alpha_c = -6.3 \times 10^{-6}$ K^{-1}. Figure 4(b) shows the volume change of β-$CuZnV_2O_7$ varying with temperature. The calculated volume expansion coefficient based on the data in Fig. 4(b) is $\alpha_v = -2.34 \times 10^{-6}$ K^{-1}. The average liner expansion coefficient obtained from the volume expansion coefficient is $\alpha_l = -0.78 \times 10^{-6}$ K^{-1}. Since the XRD reveals the intrinsic lattice variations, the low thermal expansion coefficients calculated from the XRD data suggest that β-$CuZnV_2O_7$ belongs to a near-zero thermal expansion material.

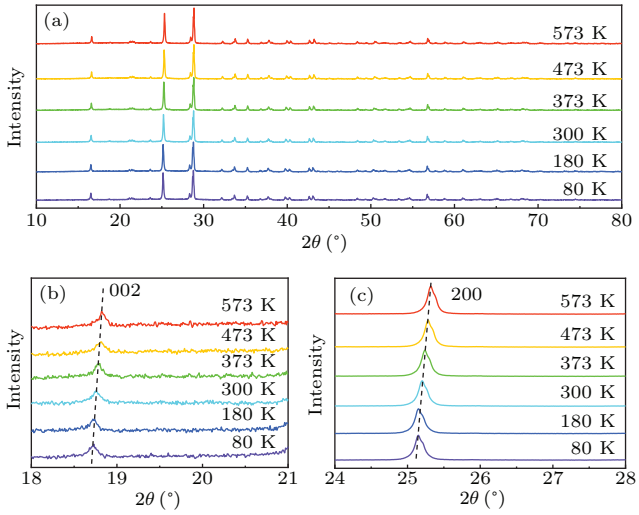

Fig. 3. (a) XRD spectra of β-$CuZnV_2O_7$ at different temperatures; (b) and (c) a partially enlarged view of temperature-dependent XRD data.

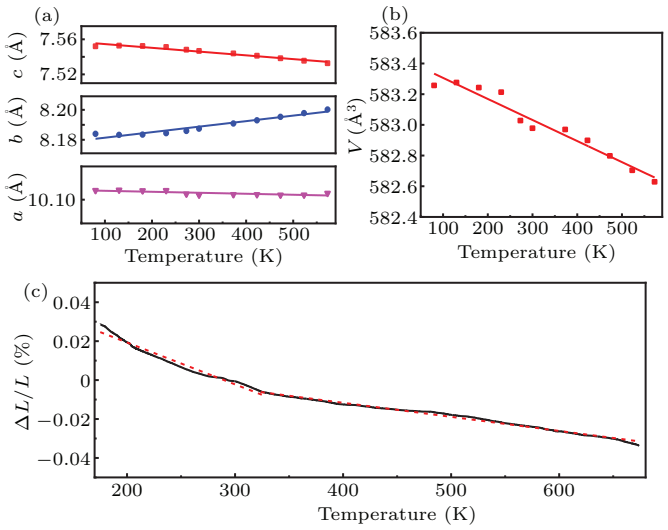

Fig. 4. (a) and (b) Changes in the lattice constants and cell volume of β-$CuZnV_2O_7$ of low-temperature XRD; (c) relative length (%) changes of the sample at temperatures from 173 K to 673 K.

The relative length change of β-$CuZnV_2O_7$ is depicted in Fig. 4(c) from 173 K to 673 K. This thermal expansion curve could be fitted well by two dotted polylines in the temperature ranges of 173–325 K and 325–673 K, resulting in two different linear thermal expansion coefficients, which are $\alpha_l = -2.15 \times 10^{-6}$ K^{-1} (173–325 K) and $\alpha_l = -0.72 \times 10^{-6}$ K^{-1} (325–673 K). The ZTE behavior of β-$CuZnV_2O_7$ is comparable with the zero expansion material of $Ta_2Mo_2O_{11}$ ($\alpha_l = 0.37 \times$

10^{-6} K^{-1}, 200–600 K), $MgZrF_6$ ($\alpha_v = -2.38 \times 10^{-6}$ K^{-1}, 300–675 K) and $TiCo(CN)_6{\cdot}2H_2O$ ($\alpha_l = -2.2 \times 10^{-8}$ K^{-1}, 100–300 K),[33–35] but with a larger ZTE temperature range. These two linear thermal expansion coefficients are different from the value ($\alpha_l = -0.78 \times 10^{-6}$ K^{-1}) obtained by the Rietveld refinement of XRD data. This deviation could be attributed to the tiny voids, holes, and micro-cracks shown in Fig. 2(a). As the thermal expansion curve measured by dilatometer represents the macroscopic properties of materials, the minor segmented linear thermal expansion coefficients also point out the near-zero expansion property of β-$CuZnV_2O_7$, which brings into correspondence with the intrinsic XRD result.

Figure 5(a) exhibits the Raman spectrum of β-$CuZnV_2O_7$ at 303 K. Our Raman results are consistent with those of $Cu_{1.5}Mg_{0.5}V_2O_7$ and β-$Cu_2V_2O_7$ above 200 cm^{-1},[25,31] which verifies the fact that β-$CuZnV_2O_7$ possesses the same structure with $Cu_{1.5}Mg_{0.5}V_2O_7$ and β-$Cu_2V_2O_7$.[18,25] This consistency supports the high quality of our sample. More detailed peaks of the spectra under 200 cm^{-1} could be detected resorting to the high resolution (0.6 cm^{-1}) and ultra-low filter of our Raman spectroscopy. The temperature-dependent Raman spectrum of β-$CuZnV_2O_7$ is shown in Fig. 5(b). The fitted peak positions of each peak in Fig. 5(b) at different temperatures are shown in Fig. 5(c). According to Fig. 5(c), all peak positions show monotonous red shifts with temperature rising and no additional peaks appear, except the peaks of 847 cm^{-1}, 796 cm^{-1}, 463 cm^{-1}, and 349 cm^{-1}, which are too broad to be fitted at high temperatures resulting from the anharmonicity of phonon. Our Raman data supports that no structural phase transition exists from 143 K to 663 K at atmospheric pressure, which is in sync with our XRD result.

As the element of Zn is adjacent with Cu in the periodic table, in β-$CuZnV_2O_7$ and β-$Cu_2V_2O_7$, the phonons with similar energy could be attributed to the similar atoms vibration modes in the Raman spectrum. The vibration modes in different energy ranges of β-$Cu_2V_2O_7$ have been identified by de Waal and Hutter. For the Raman spectra of the β-$Cu_2V_2O_7$, the Raman peaks in the regions of 350–400 cm^{-1} and 800–1200 cm^{-1} correspond to the bending vibration mode and the stretching vibration mode of the VO_4 tetrahedron, respectively; the Raman peaks in the regions of 400–550 cm^{-1} and 660–800 cm^{-1} correspond to the bridge V–O–V symmetric and anti-symmetric stretching vibration mode, respectively.[31]

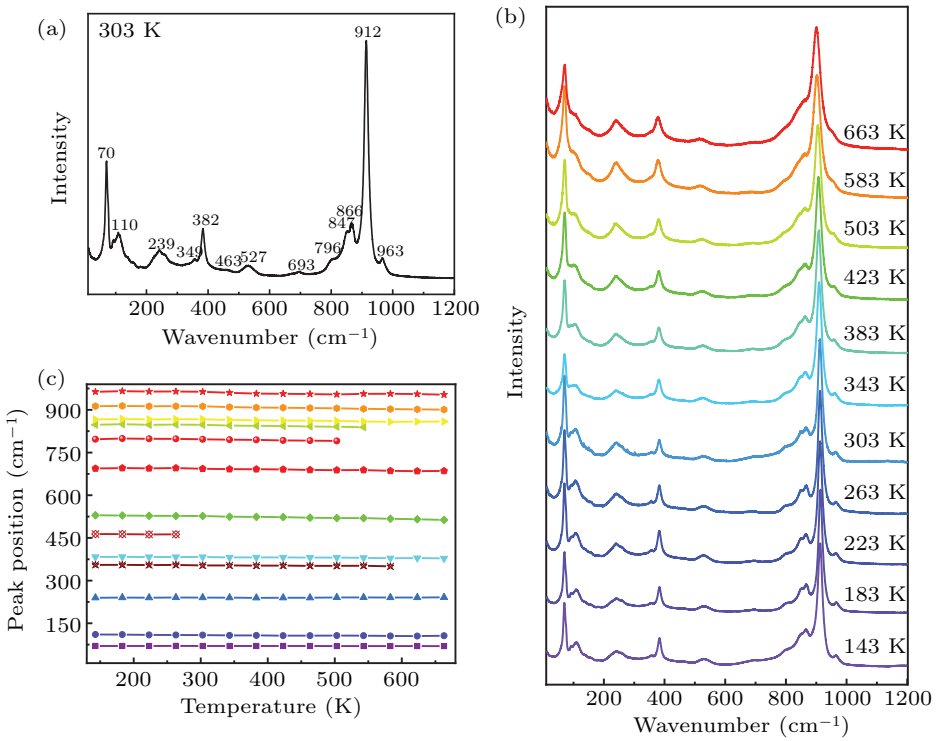

Fig. 5. (a) Raman spectra of β-$CuZnV_2O_7$ at room temperature; (b) the Raman spectrum of β-$CuZnV_2O_7$ at different temperatures; (c) the fitted phonon energies of β-$CuZnV_2O_7$ varying with temperature.

According to the identification of the Raman peaks of β-$Cu_2V_2O_7$ above, in the Raman spectrum of β-$CuZnV_2O_7$, the 349 cm^{-1} and 382 cm^{-1} peaks belong to the bending vibration of the VO_4 tetrahedron. The 847 cm^{-1}, 866 cm^{-1}, 912 cm^{-1}, and 963 cm^{-1} peaks indicate the stretching vibration mode of the VO_4 tetrahedron. The 463 cm^{-1} and 527 cm^{-1} peaks represent the V–O–V symmetrical stretching vibration. The 693 cm^{-1} and 796 cm^{-1} peaks stand for the V–O–V anti-symmetric stretching vibration. Furthermore, though the peaks 70 cm^{-1}, 110 cm^{-1}, and 239 cm^{-1} were not indexed

to any atomic vibrations previously, we infer them to be translational and librational movements of the VO_4 tetrahedron empirically. Because in many other NTE compounds with open framework structures, Raman modes at below 280 cm^{-1} can be identified as translational and librational vibrations of tetrahedra, such as $Zr_{0.3}Sc_{1.7}Mo_{2.7}V_{0.3}O_{12}$, $HfMgW_3O_{12}$, and $Zn_2V_{1.7}P_{0.3}O_7$.[36–38]

3.4. Two structural phase transitions under high-pressure and the mechanism of NTE

To improve the understanding of the NTE mechanism in β-$CuZnV_2O_7$, a high-pressure Raman experiment has been carried out to acquire the contribution of phonon anharmonicity to NTE properties. Figure 6(a) shows the pressure-dependent Raman spectra. The peaks labeled by the diamond marker are not the Raman signals of β-$CuZnV_2O_7$ but silicon oil which is the pressure transmitting medium. As is well known, the discontinuous changes in Raman peaks demonstrate the structure changing. Apparently, two structural phase transitions exist as pressure varying from 0 to 7.84 GPa. The first phase transition appears at 0.94 GPa, symbolized by the distinct differences of the Raman peaks marked by the inverted triangle from 800–1000 cm^{-1}, where the number and the shape of peaks have changed none monotonously. The second phase transition happens at 6.35 GPa, which could be revealed by the appearance of the peak at about 850 cm^{-1} denoted by the circle.

To get insight into the mechanisms of NTE in β-$CuZnV_2O_7$, the mode Grüneisen parameter γ_i is a powerful medium to know more about the thermal property of materials,[39,40]

$$\alpha_V = \frac{k_B}{3VB_0}\sum_i p_i\gamma_i\left(\frac{\hbar\omega_i}{k_BT}\right)\exp\left(\frac{\hbar\omega_i}{k_BT}\right) \times\left[\exp\left(\frac{\hbar\omega_i}{k_BT}\right)-1\right]^{-2}, \quad (1)$$

where ω_i is the frequency of the ith mode, V is the molar volume, B_0 is the bulk modulus, k_B is the Boltzmann constant, and p_i is the degeneracy of the phonon mode with frequency ω_i at the Brillouin zone center.

In Eq. (1), the sign of α_V is totally determined by γ_i. That is to say, if the material behaves NTE property, where α_V is negative, the γ_i should be minus, and vice versa. The Grüneisen parameter γ_i could be obtained through formula

$$\gamma_i = (\omega_i x_T)^{-1}\left(\frac{\partial\omega_i}{\partial P}\right), \quad (2)$$

where ω_i is Raman frequency of the mode i, P is the pressure, and x_T is the isothermal volume compressibility. The sign of γ_i is completely decided by the sign of $\partial\omega_i/\partial P$. If the phonon energy decreases with increasing pressure, the sign of $\partial\omega_i/\partial P$ would be negative.

In our case, from 0 to 0.57 GPa, most of the Raman peaks exhibit blue shifts, which is a regular behavior resulting from the shortening of bond length as pressure increasing, except for the 69 cm^{-1}, 352 cm^{-1}, and 526 cm^{-1} peaks. Each $\partial\omega_i/\partial P$ of the 69 cm^{-1}, 352 cm^{-1}, and 526 cm^{-1} peaks is minus according to the data in Fig. 6(b), where the energy of each Raman peak tends to decrease with pressure rising. Thus, the corresponding Grüneisen parameters of 69 cm^{-1}, 352 cm^{-1}, and 527 cm^{-1} peaks are all negative, indicating that these three Raman modes give a major contribution to the NTE characteristic of β-$CuZnV_2O_7$.

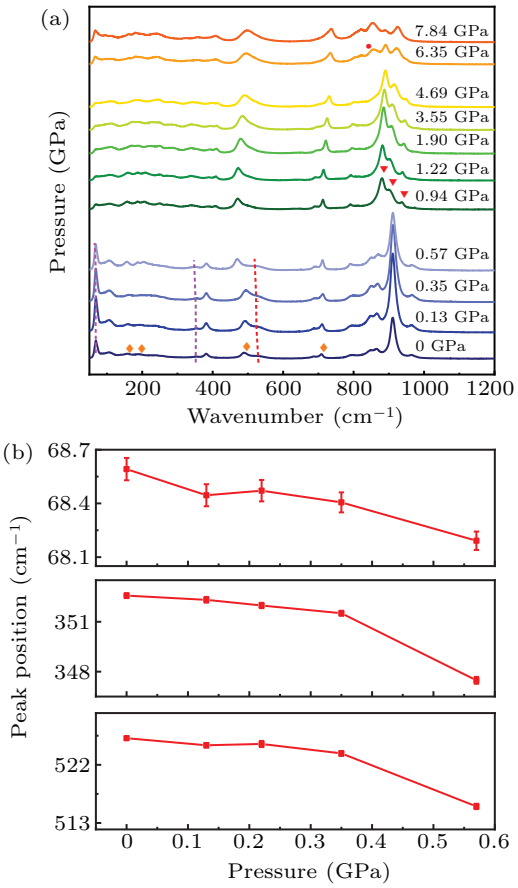

Fig. 6. (a) Raman spectra of β-$CuZnV_2O_7$ at different pressures; (b) Raman mode frequency shifts as a function of pressure.

Compared to the phonon anharmonicity, the variation of bond angle varying with temperature could provide a more direct approach to uncover the NTE mechanism in β-$CuZnV_2O_7$. Figure 7 shows the temperature dependence of the angles between Cu(Zn)–O_2–V, Cu(Zn)–O_3–V, and V–O–V, respectively, obtained by the Rietveld refinement based on the low-temperature XRD data in Fig. 3(a). As the temperature rises, the lateral vibration of the bridge oxygen atoms shared by the VO_4 tetrahedron and the $(CuZn)_{0.5}O_5$ pentahedron increases, resulting in a gradual decrease in the angle between Cu(Zn)–O_3–V and Cu(Zn)–O_2–V, which makes a great contribution to the negative thermal expansion of the crystal axes a and c. The insets in Figs. 7(a) and 7(b) give a more intuitive

manner to observe the reducing of the a and c axes. Unlike the decreasing of angle above, the angle between V–O–V gains as pressure increasing, which is counterintuitive. According to our high-pressure Raman result given above, the η peak contributes greatly to the NTE property of β-$CuZnV_2O_7$. Based on our analysis of the atoms vibrations in Raman experiment mentioned above, this peak represents the V–O–V symmetrical stretching vibration, which would lead to rising of the angle between V–O–V as shown by the vibration sketch of atoms in Fig. 7(c). Therefore, this increase of the angle between V–O–V could also give a significant contribution to the NTE of β-$CuZnV_2O_7$.

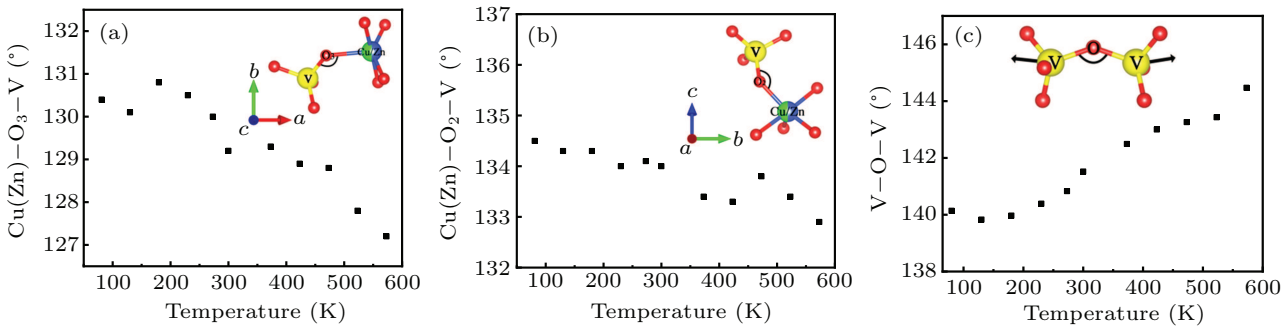

Fig. 7. Angles of (a) Cu(Zn)–O_3–V, (b) Cu(Zn)–O_2–V, and (c) V–O–V varies with temperature. The insets are schematics of (a) angle of Cu(Zn)–O_3–V in a direction, (b) angle of Cu(Zn)–O_2–V in c direction, and (c) probable schematic diagram of the V–O–V symmetrical stretching vibration, which is just a qualitative representation of the vibration mode.

4. Conclusion and perspectives

In our experiment, a solid phase reaction method is used to synthesize the polycrystal powder of β-$CuZnV_2O_7$. Both of the temperature-dependent XRD and Raman experiments reveal that no structural phase transition exists at atmospheric pressure. However, detailed high-pressure Raman data suggests that two structural phase transitions happen at 0.94 GPa and 6.35 GPa, respectively, manifested as anomalous changes in the position and quantity in phonon peaks. The macroscopic linear thermal expansion coefficient obtained by the dilatometer is $\alpha_l = -2.15 \times 10^{-6}$ K^{-1} (173–325 K) and $\alpha_l = -0.72 \times 10^{-6}$ K^{-1} (325–673 K), which is almost consistent with the intrinsic linear thermal expansion $\alpha_l = -0.78 \times 10^{-6}$ K^{-1}. This consistency declares that the β-$CuZnV_2O_7$ belongs to a near-zero NTE material with a large NTE temperature range from 173 K to 673 K. The XRD data supports the decrease of a and c axes with the increasing temperature, which could be demonstrated expressly by the schematic diagrams. The negative Grüneisen parameters indicate that the anharmonicity of 69 cm^{-1}, 352 cm^{-1}, and 527 cm^{-1} peaks gives a great contribution to the NTE characteristics in β-$CuZnV_2O_7$. The atomic vibration of the 527 cm^{-1} peak explains why the increase of the angle between V–O–V could lead to the shortening of volume in β-$CuZnV_2O_7$ upon temperature increasing. This work provides not only detailed insights into the structure and the NTE mechanism in β-$CuZnV_2O_7$ but also important significance for understanding the NTE in other framework materials.

Acknowledgements

This work was supported by the National Natural Science Foundation of China (Grant Nos. 11874328, 12004339, 11574276, and 21905252), the China Postdoctoral Science Foundation (Grant Nos. 2018M640679, 2019T120629, and 2019M652558), and the Zhongyuan Academician Foundation (Grant No. ZYQR201810163).

References

[1] Liang E J, Sun Q, Yuan H L, Wang J Q, Zeng G J and Gao Q L 2021 *Front. Phys.* **16** 53302
[2] Gao Q L, Wang J, Sanson A, Sun Q, Liang E J, Xing X R and Chen J 2020 *J. Am. Chem. Soc.* **142** 6935
[3] Ge X H, Mao Y C, Li L, Li L P, Yuan N, Cheng Y G, Guo J, Chao M J and Liang E J 2016 *Chin. Phys. Lett.* **33** 046503
[4] Liu F S, Chen X P, Xie H X, Ao W Q and Li J Q 2010 *Acta Phys. Sin.* **59** 3350 (in Chinese)
[5] Xu S, Hu Y M, Liang Y, Shi C F, Su Y L, Guo J, Gao Q L, Chao M J and Liang E J 2020 *Chin. Phys. B* **29** 086501
[6] Hummel F A 2010 *J. Am. Ceram. Soc.* **34** 235
[7] Poowancum A, Matsumaru K and Ishizaki K 2011 *J. Am. Ceram. Soc.* **94** 1354
[8] Duan N, Kameswari U and Sleight A W 2013 *J. Am. Chem. Soc.* **121** 10432
[9] Marinkovic B A, Jardim P M, Avillez R R Rizzo F 2005 *Solid State Sci.* **7** 1377
[10] Evans J S O, Mary T A, Vogt T, Subramanian M A and Sleight A W 1996 *Chem. Mater.* **8** 2809
[11] Khosrovani N, Sleight A W and Vogt T 1997 *J. Solid State Chem.* **132** 355
[12] Mary T A, Evans J S O, Vogt T and Sleight A W 1996 *Science* **272** 90
[13] Evans J S O, Hanson J C and Sleight A W 1998 *Acta Crystall.* **54** 705
[14] Mittal R, Chaplot S L 2008 *Phys. Rev. B* **78** 174303
[15] Turquat C, Muller C, Nigrelli E, Soubeyroux J L and Nihoul G 2000 *Eur. Phys. J. AP* **10** 15
[16] Hisashige T, Yamaguchi T, Tsuji T and Yamamura Y 2006 *J. Ceram. Soc. Jpn.* **114** 607
[17] Zhang N, Li L, Wu M Y, Li Y X, Feng D S, Liu C Y, Mao Y C, Guo J, Chao M J and Liang E J 2016 *J. Eur. Ceram. Soc.* **36** 2761
[18] Wang H, Yang M J, Guo J, Gao Q L, Jiao Y J, Tang X B, Chao M J and Liang E J 2019 *Solid State Ionics* **343** 115086
[19] Krasnenko T, Medvedeva N and Bamburov V 2010 *Adv. Sci. Technol.* **63** 358
[20] Krasnenko T I, Zolotukhina L V and Andrianova L V 2000 *Inorg. Mater.* **36** 1032

[21] Rotermel M V and Krasnenko T I 2017 *Crystall. Rep.* **62** 703
[22] Shi N K, Sanson A, Gao Q L, Sun Q, Ren Y, Huang Z H, Souza D O, Xing X R and Chen J 2020 *J. Am. Chem. Soc.* **142** 3088
[23] Yuan H L, Yuan B H, Fang L and Liang E J 2012 *Acta Phys. Sin.* **61** 226502 (in Chinese)
[24] Wei W, Gao Q, Guo J, Chao M J, He L H, Chen J and Liang E J 2020 *Appl. Phys. Lett.* **116** 181902
[25] Wang H, Yang M J, Chao M, Guo J, Tang X B, Jiao Y J and Liang E J 2019 *Ceram. Int.* **45** 9814
[26] Katayama N, Otsuka K, Mitamura M, Yokoyama Y, Okamoto Y and Takenaka K 2018 *Appl. Phys. Lett.* **113** 181902
[27] Wang J P, Chen Q D, Li S L, Ji Y J, Mu W Y, Feng W W, Zeng G J, Liu Y W and Liang E J 2018 *Chin. Phys. B* **27** 066501
[28] He X K, Qi H, Xu Q, Liu X S, Xu L and Yuan B H 2016 *Chin. Phys. B* **28** 056501
[29] Rotermel M V, Krasnenko T I, Petrova S A and Titova S G 2018 *Chim. Technol. Acta* **5** 86
[30] Shi N K, Sanson A, Venier A, Fan L L, Sun C J, Xing X R and Chen J 2020 *Chem. Commun.* **56** 10666
[31] Waal D and Hutter C 1994 *Mater. Res. Bull.* **29** 843
[32] Schindler M and Hawthorne F C 1999 *J. Solid State Chem.* **146** 271
[33] Gao Y X, Wang C Y, Gao Q L, Guo J, Chao M J, Jia Y and Liang E J 2020 *Inorg. Chem.* **59** 18427
[34] Xu J L, Hu L, Song Y Z, Han F, Qiao Y Q, Deng J X, Chen J and Xing X R 2017 *J. Am. Ceram. Soc.* **100** 5385
[35] Gao Q L, Shi X W, Venier A, Carnera A, Huang Q Z, Wu H, Chen J, Sanson A and Liang E J 2020 *Inorg. Chem.* **59** 14852
[36] Zeng G J, Yuan H L, Guo J, Sun Q, Gao Q L, Chao M J, Ren X and Liang E J 2020 *Phys. Chem. Chem. Phys.* **22** 12605
[37] Yuan H L, Wang C Y, Gao Q L, Ge X H, Sun H, Lapidus S H, Guo J, Chao M J, Jia Yu and Laing E J 2020 *Inorg. Chem.* **59** 4090
[38] Zhu Y W, Chen R, Chen L, Chao M J, Guo J, Gao Q L and Laing E J 2021 *Solid State Sci.* **112** 106515
[39] Lucazeau G 2003 *J. Raman Spectrosc.* **34** 478
[40] Ding P, Liang E J, Jia Y and Du Z Y 2008 *J. Phys. Condens. Matter.* **20** 275224